ATMOSPHERIC SCIENCE

The impact of emissions controls on atmospheric nitrogen inputs to Chinese river basins highlights the urgency of ammonia abatement

Sijie Feng[1,2], Mengru Wang[2], Mathew R. Heal[3], Xuejun Liu[1], Xueyan Liu[4], Yuanhong Zhao[5], Maryna Strokal[2], Carolien Kroeze[2], Fusuo Zhang[1], Wen Xu[1]*

Excessive nitrogen (N) deposition affects aquatic ecosystems worldwide, but effectiveness of emissions controls and their impact on water pollution remains uncertain. In this modeling study, we assess historical and future N deposition trends in Chinese river basins and their contributions to water pollution via direct and indirect N deposition (the latter referring to transport of N to water from N deposited on land). The control of acid gas emissions (i.e., nitrogen oxides and sulfur dioxide) has had limited effectiveness in reducing total N deposition, with notable contributions from agricultural reduced N deposition. Despite increasing controls on acid gas emissions between 2011 and 2019, N inputs to rivers increased by 3%, primarily through indirect deposition. Simultaneously controlling acid gas and ammonia emissions could reduce N deposition and water inputs by 56 and 47%, respectively, by 2050 compared to 2019. Our findings underscore the importance of agricultural ammonia mitigation in protecting water bodies.

INTRODUCTION

Over the past several decades, human activities associated with energy and food production have greatly increased the availability of reactive nitrogen (Nr) in Earth's ecosystems (*1*, *2*). Atmospheric Nr predominantly comprises ammonia (NH_3) and nitrogen oxides [NO_x = nitric oxide (NO) + nitrogen dioxide (NO_2)] and enters natural and semi-natural ecosystems in the form of reduced (NH_x) and oxidized (NO_y) atmospheric deposition, respectively (below, we use NH_3 and NO_x when referring to emissions, and NH_x and NO_y when referring to deposition) (*3*). Excessive atmospheric N deposition (hereon the term N deposition means Nr deposition) has adverse impacts on the soil and water chemistry of terrestrial and aquatic ecosystems (*4*, *5*), including soil acidification (*6*), increased nutrient transport by rivers to sub-basins (*7*) and coastal waters (*8*), eutrophication (*9*), and biodiversity loss (*10*).

Aquatic ecosystems are sensitive to external N inputs, and global water quality has been adversely affected by increased N in rivers (*11*, *12*). The United Nations (UN) lists "Clean Water and Sanitation" and "Life Below Water" among its Sustainable Development Goals (SDGs) (*13*). As a consequence of intensive human activities, atmospheric N deposition has become a notable source of N in inland water in some regions (*7*, *9*, *14*, *15*). For example, N deposition sources contributed approximately 35% to the dissolved inorganic N (DIN) in China in 2012 (*16*), and N deposition accounted for over half the N inputs in 49% of watersheds in the United States in 2008–2009 (*17*). Meanwhile, the proportion of N deposition to total N loads increased to 27 to 48% in summer in Lake Dianchi (the sixth largest freshwater lake in China) in 2010–2011 (*9*). Atmospheric Nr contributes to aquatic N directly by deposition to open-water bodies (direct N deposition) or indirectly via increasing the N transported from watershed soils to nearby waterbodies (indirect N deposition) (*18*). Existing studies in China have separately focused on the impacts of direct N deposition on water bodies (*15*) or the indirect N deposition transport from land to rivers at a sub-basin scale (*7*, *14*, *16*). The latter has been achieved by applying water quality models, such as the Chinese Model to Assess River Inputs of Nutrients to Seas (MARINA-Nutrients, versions 1.0, 2.0, and 3.0). However, these models often do not account for the contribution from direct N deposition on water bodies. They also rely on the application of national average N deposition to quantify the indirect N deposition in the models due to the absence of high-resolution simulated/monitored N deposition data for each sub-basin. Evaluation of the combined impacts of direct and indirect N deposition on water pollution has not yet been undertaken. Chemical transport models (CTMs) that incorporate N emission sources and simulate the physical and chemical processes of atmospheric N pollution have been implemented at global (*19*) and national scales (*20*–*22*), which can simulate the direct N deposition on water and land at grid scale. Here, we couple the calculated N depositions on land and water from a CTM as input to a water quality model to understand the trends in the direct and indirect N deposition contributions to water pollution in China.

N deposition in China is the highest in the world, with atmospheric bulk N deposition (i.e., the sum of wet deposition and part of dry deposition) nearly doubling between the 1980s and 2010s (*1*). In partial response to these challenges, the Chinese government has implemented various policies over recent decades to control NO_x emissions, which are an important source of N deposition (*19*, *23*). However, there has been no corresponding implementation of policy to reduce emissions of NH_3 (*24*, *25*), which are another crucial source of N deposition. According to Xu *et al.* (*26*), NH_3 emissions from fertilizer application and livestock accounted for nearly half

[1]State Key Laboratory of Nutrient Use and Management, College of Resources and Environmental Sciences, Key Laboratory of Plant–Soil Interactions, Ministry of Education, National Observation and Research Station of Agriculture Green Development (Quzhou, Hebei), China Agricultural University, Beijing 100193, China. [2]Earth Systems and Global Change Group, Wageningen University & Research, Wageningen 6708 PB, Netherlands. [3]School of Chemistry, The University of Edinburgh, Edinburgh EH9 3FJ, UK. [4]School of Earth System Science, Tianjin University, Tianjin 300072, China. [5]College of Oceanic and Atmospheric Sciences, Ocean University of China, Qingdao 266100, China.
*Corresponding author. Email: wenxu@cau.edu.cn

(46%) of the total inorganic Nr deposition across eastern China. In addition, the influence of meteorology (e.g., precipitation) and the lag between emissions and deposition (*27*) mean that the effectiveness of current policies to control N deposition to inland water, if any, remains unclear. It is therefore essential to determine the sources and relative contributions of N deposition to inland water so as to develop effective strategies for mitigation of its impacts.

Our aims here are to: (i) examine long-term (1990s to 2010s) trends and spatial distributions of N deposition via different pathways (wet and dry) and in various chemical forms (NH_x and NO_y) in 33 Chinese sub-basins (fig. S1), (ii) assess the impacts of the implemented emission control policies on N deposition during the last three decades and the anticipated changes in N deposition in the future (2050), and (iii) evaluate the effects on N inputs to rivers from current (2010s) and future (2050) direct and indirect N deposition. To do so, we first applied the GEOS-Chem CTM at 0.5° × 0.625° spatial resolution over China to simulate N deposition on land and rivers directly by source for six target years representing the 1990s to 2010s (specifically: 1991, 1999, 2001, 2009, 2011, and 2019). In addition, we simulated N deposition for the year 2050 using optimal anthropogenic emissions. We then coupled GEOS-Chem with the MARINA-Nutrients model (version 2.0) to quantify N inputs to rivers from direct and indirect N deposition over the sub-basins in 2011, 2019, and 2050. The research framework for this study is shown in fig. S2. Our results improve our understanding of the effects of historical atmospheric policies on N pollution abatement in Chinese sub-basins and help identify a scientific basis for curbing N deposition in sensitive aquatic ecosystems.

RESULTS AND DISCUSSION

N deposition across three decades

We used the GEOS-Chem model to quantify the annual total N deposition to the 33 Chinese sub-basins across three decades from the wet and dry depositions of the individual contributing species: NH_x, comprising ammonium (NH_4^+) and NH_3; and NO_y, comprising nitrate (NO_3^-), nitric acid (HNO_3), NO_2, and other NO_y gases (fig. S3 and table S1). Between 1991 and 2019, the mean total N deposition ($NH_x + NO_y$) to these river basins increased by 55%, reaching 23.7 kg N ha^{-1} $year^{-1}$ in 2019 (Fig. 1 and table S1). The increase in mean total N deposition was notably greater to the southern river basins (Hanjiang, Jiulong, Menjiang, Oujiang, Fuchun, Pearl, and Yangtze) (77%) than to the northern river basins (Yellow, Huai, Hai, Liao, Yalu, and Luan) (18%). The 55% increase in mean total N deposition in China far exceeded the world average increase of 8% over a similar period (*28*). Our results for 1991 to 2011 are consistent with previous reports of long-term increasing N deposition in China (*19*, *29*). The mean total N deposition in this study for 2011 (21.2 kg N ha^{-1} $year^{-1}$) closely matches the value reported by Yu *et al.* (*29*) for the period 2011 to 2015 (21 kg N ha^{-1} $year^{-1}$).

The NO_y deposition more than doubled on average across the 33 sub-basins during the 1990s and 2000s, reaching 12.6 kg N ha^{-1} $year^{-1}$ in 2011 before decreasing to 11.3 kg N ha^{-1} $year^{-1}$ in 2019 (fig. S4A), mirroring the trend observed in NO_x emission from 1991 to 2019 (fig. S5C). Specifically, between 1991 and 2011, the southern and northern river basins experienced increases in NO_y deposition of 118% (from 6.2 to 13.5 kg N ha^{-1} $year^{-1}$) and 77% (from 6.2 to 11.0 kg N ha^{-1} $year^{-1}$), respectively (fig. S6A). Between 2011 and 2019, NO_y deposition to the southern river basins did not change, while it reduced by 25%, on average, to the northern river basins. In contrast, NH_3 emissions remained around 8 Tg N $year^{-1}$ during the last three decades (fig. S5B), causing average NH_x deposition across the 33 sub-basins remained constant at around 9 kg N ha^{-1} $year^{-1}$ between 1991 and 2011 but with an increase to 12.4 kg N ha^{-1} $year^{-1}$ in 2019 (fig. S4B). Most of this increase in NH_x deposition occurred in the southern river basins: On average, NH_x deposition in these basins increased by 59% (from 7.5 to 11.9 kg N ha^{-1} $year^{-1}$) between 2011 and 2019 (fig. S6A). The differences in deposition amounts and trends between northern and southern river basins are explained by both human activities (*29*) and meteorological conditions (*27*). The substantial variations in NH_x deposition in southern river basins can be attributed to dense agricultural activities, such as livestock density (*30*) and fertilizer application (*31*). In addition, the high precipitation over the southern river basins (fig. S7) is very effective at removing water-soluble gaseous pollutants and aerosol particles from the atmosphere (*32*), increasing the NH_x deposition in these basins.

Our results from the sensitivity test 1 (ST1) model simulations show that anthropogenic emissions were the dominant contributors to the decadal variations in total N deposition (1990s: 103%; 2000s: 88%; 2010s: 89%; fig. S5A). Nevertheless, note that the 2000s and 2010s were, respectively, subjected to 12 and 11% increases in total N deposition due to changes in meteorology only (fig. S5A), which could lead to lags in observing responses of, for example, NO_y deposition, to policy implementations (*27*). Therefore, to understand the policy-driven anthropogenic effects on N deposition, it is necessary to simulate using fixed meteorological conditions, as described in the following section.

N deposition response to the implementation of policies and current source contributions

Figures S5, S8, and S9 summarize the spatial and temporal changes in N deposition in each decade when using actual meteorology and when using fixed meteorology in each decade (the ST1 simulations). The total N deposition fluxes resulting from human activities only increased by 18.3% in the 1990s, decreased by 2.7% in the 2000s, and increased by 0.5% in the 2010s (fig. S9). The responses of N deposition over these decades can be discussed in the context of the timeline of air pollution and agricultural policies in China shown in fig. S10.

At the beginning of the 1990s, intensive industrial expansion led to an increase in NO_x and sulfur dioxide (SO_2) emissions, resulting in increased NO_y deposition during this decade (fig. S5C), especially in the southern river basins (fig. S8A). Before the mid-1990s, intensive agricultural activities also increased NH_3 emissions and NH_x deposition. However, the implementation of agricultural policies to reduce the use of N fertilizer and improve the N use efficiency (fig. S10) (*29*), together with the Asia financial crisis in 1997 (*33*), led to reductions in both livestock numbers and synthetic fertilizer industries and to no net change in NH_x deposition in the 1990s (fig. S5B).

In the 2000s, emission controls of vehicles and industry caused NO_x emissions to decrease slightly (by 1.2% between 2001 and 2009) (fig. S5C), leading to a slight reduction (2.7%) in total N deposition from human activities (fig. S9). Although China's coal-based energy structure and rapid growth of energy consumption contributed to substantial SO_2 and NO_x emissions before 2005, effective measures were taken to reduce emissions of these acid gases after 2006.

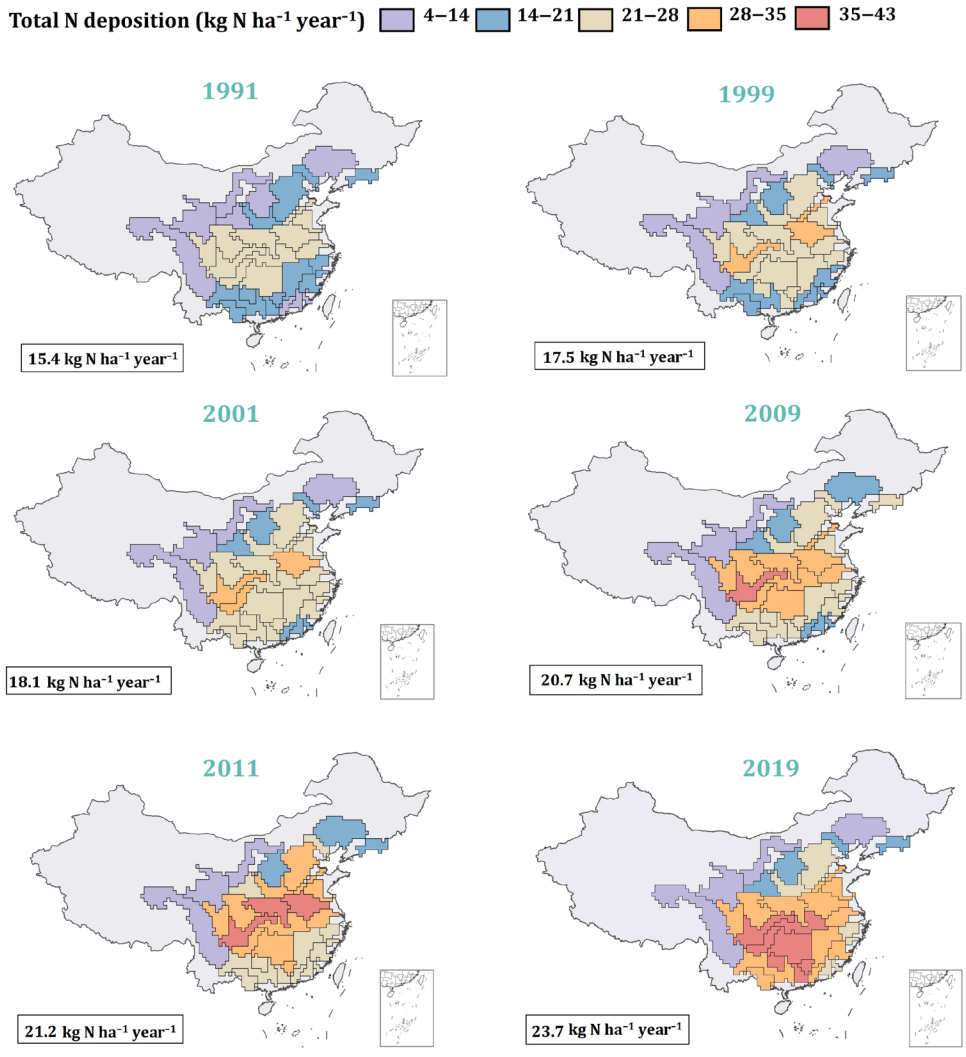

Fig. 1. Modeled annual total N deposition to land in 33 Chinese sub-basins for six years (1991, 1999, 2001, 2009, 2011 and 2019) spanning three decades (1990s, 2000s, and 2010s) (unit: kg N ha^{-1} yr^{-1}) using GEOS-Chem at 0.5° × 0.625° horizontal resolution. The boxed numbers are the average total N deposition to land across all 33 sub-basins in the given year. The depositions from oxidized N (NO_y) and reduced N (NH_x) separately are shown in fig. S4.

Consequently, NO_y deposition declined in China from 2006 to 2010 (*27*). The lack of notable changes in NH_x deposition during the 2000s (fig. S5B) can be explained by atmospheric chemistry. There is a preferential and nonreversible reaction of NH_3 with sulfuric acid (H_2SO_4) compared with its reversible reaction with HNO_3 or hydrogen chloride (HCl). When SO_2 is high, the deposition of NH_x is decreased because less is present as NH_3, which has a higher deposition velocity than particulate N (*29*). Thus, in the 2000s, a decline in NH_x deposition due to rising SO_2 emissions during the first part of the decade was counterbalanced by an increase in NH_x deposition caused by the reductions in SO_2 emissions in the latter part. Concurrent implementation of agricultural NH_3 emission management measures (such as implemented discharge standard of pollutants of livestock and poultry breeding, and proposed the Soil Testing and Fertilizer Recommendation Project) also played a role in limiting the growth of NH_x deposition (fig. S10).

From the 2010s onward, more stringent policies were implemented to jointly control both NO_x and SO_2 emissions and improve air quality (fig. S10), leading to a substantial decrease (24%) in NO_x emissions from human activities between 2011 and 2019 (fig. S5C). A previous study also showed that implementation of the Action Plan in China reduced NO_x emissions nationally by 21% from 2013 to 2017 (*34*). The positive effects of these measures on N deposition to river basins are illustrated in our work: NO_y deposition from human activities to the river basins decreased by 2.4 kg N ha^{-1} year^{-1} between 2011 and 2019 (table S2), and the NO_y proportion of the total N deposition decreased by 12% during this period (Fig. 2). The decrease in NO_y deposition after 2011 shown here is consistent with previous modeling and empirical studies (*19*, *23*) and further confirms that strict emission control led to reductions in NO_y deposition in the 2010s (fig. S5C). The reductions in NO_y deposition include a reduction in dry deposition of HNO_3 (−7%) (Fig. 2) and in other dry-deposited species that are particularly sensitive to changes in emissions (*27*). However, the decrease in NO_y deposition was offset by increased NH_x deposition (fig. S5B), leading to no notable reduction in total N deposition during the decade (0.5% increase in total

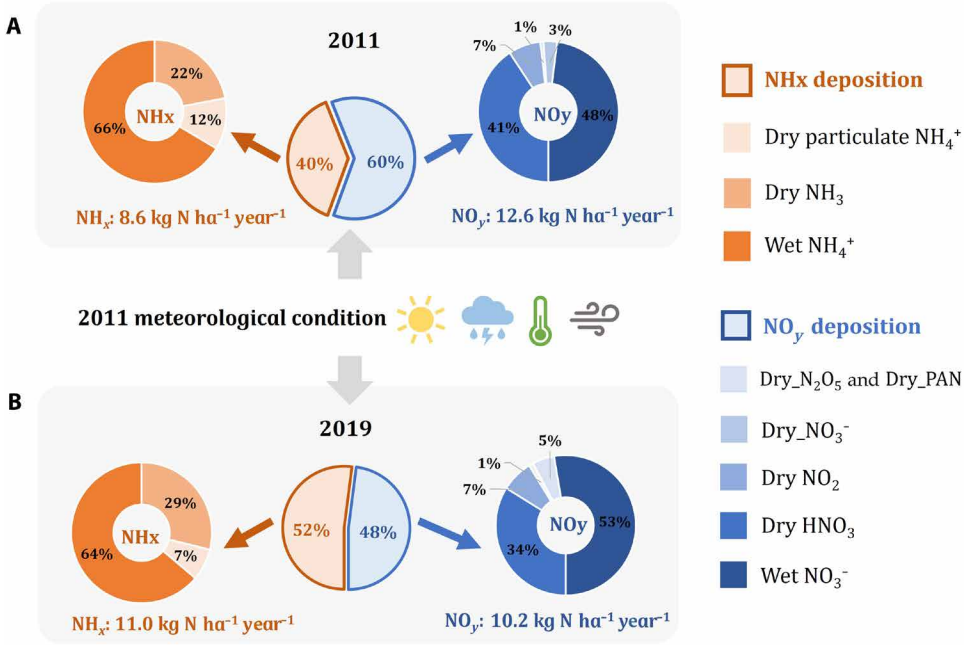

Fig. 2. Average contributions of different species of nitrogen (N) to total N deposition in 33 Chinese sub-basins in the 2010s under the same meteorology. (**A**) The year of 2011 and (**B**) the year of 2019. The results derive from the ST1 simulations using the GEOS-Chem model.

N deposition from human activities in the 2010s) (fig. S9). Our results show that the contribution of NH_x deposition to total N deposition increased from 40% in 2011 to 52% in 2019 (Fig. 2), becoming the larger component of total N deposition. The increase in NH_x deposition is primarily driven by the increases in wet NH_4^+ deposition ($\Delta = 1.3$ kg N ha^{-1} $year^{-1}$) and dry NH_3 deposition ($\Delta = 1.3$ kg N ha^{-1} $year^{-1}$) (table S2).

Our sensitivity test 2 (ST2) enable us to determine the sources of the changes in NH_x and NO_y deposition in the 2010s. Figure 3 illustrates the fractional contributions of six emission sectors to the total N deposition over the 33 Chinese sub-basins in 2011 and 2019. During the 2010s, agriculture was the main contributor to total N deposition, with its fractional contribution increasing by 7 percentage points from 30% in 2011 to 37% in 2019, while fractional contributions from power plants and residential decreased by 8 percentage points and 5 percentage points, respectively. The substantial reductions in atmospheric concentrations of SO_2 and NO_2 (fig. S11), brought about by policy controls on power plant and residential source (*34*), coupled with insufficient N management in agriculture (*30*, *35*) and spillover effects of strictly controlled areas (such as Beijing-Tianjin-Hebei) (*36*) mean that NH_3 concentrations have been increasing (*23*, *29*). Meanwhile, a comparison of the spatial variation in changes of contributing emission sectors between 2011 and 2019 (fig. S12) shows that the northern sub-basins experienced greater decreases in contributions from the residential sector (average decrease of 6 percentage points) compared to the southern sub-basins (average decrease of 3 percentage points). These results reveal the positive impacts on N deposition in northern China resulting from the substitution of direct coal burning with electricity and natural gas (*34*). In contrast, the southern basins experienced a 7 percentage points increase in the contribution to N deposition from agricultural sources, compared to a 5 percentage points increase in northern river basins. This can be attributed to the more intensive agricultural production in the south area. For example, national N fertilizer data shows that the average amount of applied N fertilizer in southern China was higher than that in northern China (fig. S13B). Given the considerable current impact of NH_3 emissions on N deposition, it is important to prioritize better N management practices within agriculture in the future (*37*).

Therefore, we conducted a modeling analysis to assess the potential benefits of implementing acid emissions control alongside strict regulation of agricultural NH_3 emissions [sensitivity test 3 (ST3)] on future N deposition in the 33 Chinese sub-basins. We used the comprehensive future scenario developed by Tong *et al.* (*38*), which encompass diverse sectors such as power, industry, residential, transportation, and agriculture (table S3). This scenario aims for optimal economic growth while prioritizing a clean environment and public health in China by 2050, and the future scenario is described in detail in ST3 of Materials and Methods. The changes in total SO_2, NH_3, and NO_x emissions in China in 2050 compared to 2011 and 2019 are shown in fig. S14. The projections indicate that by 2050, the total N deposition from human activities in 33 Chinese sub-basins is expected to decline to 9.3 kg N ha^{-1} $year^{-1}$, representing a 56% decline compared to the levels modeled during the 2010s (Fig. 4). Specifically, compared to the emissions changes observed between 2050 and the 2019 (averaging a 54% decrease), the reduction in NO_y deposition by 58% aligns with the decrease in NO_x emissions. This correspondence suggests a direct influence of anthropogenic emissions on future NO_y deposition through changes in NO_x emissions. However, the average 27% decrease in NH_3 emissions is anticipated to lead to a 51% reduction in NH_x deposition, with notable decreases observed in some southern sub-basins such as Jinsha and Jialing, where the NH_x deposition is expected to decrease by 70 and 60%, respectively. Our findings underscore the

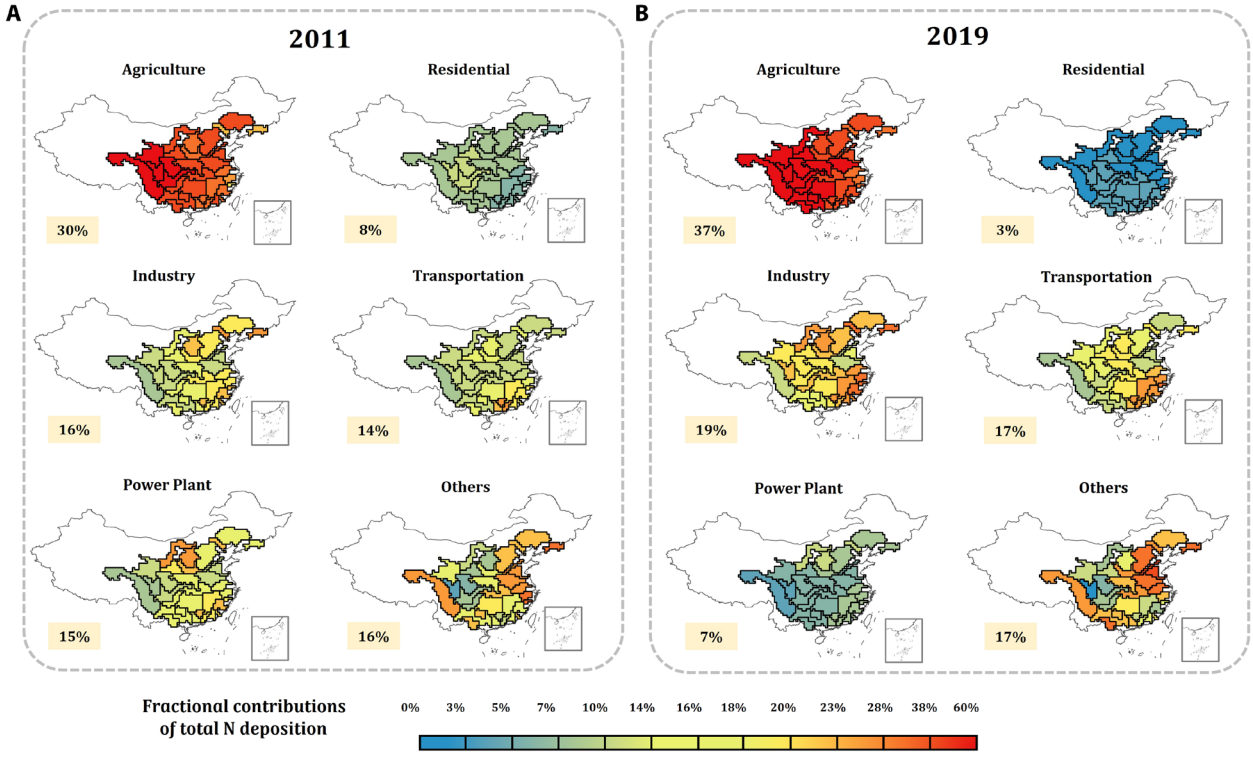

Fig. 3. Fractional contributions of six emission sectors to total N deposition in each of the 33 Chinese sub-basins in the 2010s. (**A**) Year of 2011 and (**B**) the year of 2019. The emission sectors are agriculture, industry, power plant, residential, transportation, and others (includes transboundary sources, soil, lightning, and biomass burning). The numbers in the boxes are the average contribution of each source across all sub-basins. The results derive from the ST2 simulations using the GEOS-Chem model.

notable impact of emission control measures in the agricultural sector, including intensified cultivation, grazing management enhancements, and the promotion of slow-release fertilizer (table S3) in achieving substantial reductions in total N deposition in the future (fig. S14).

Impacts of current and future N deposition on water pollution

Figure 5 shows the quantification of the contributions of direct and indirect N deposition on water pollution in the 33 sub-basins in this study. Direct N deposition refers to N deposition on water directly; indirect N deposition refers to the transportation of N to water from N deposition on land. Our findings reveal that indirect N deposition accounted for 77 to 99% of N inputs to rivers from N deposition between 2011 and 2019. N inputs to rivers from direct and indirect deposition were 289 and 3901 kiloton (kton) in 2011 and 311 and 4472 kton in 2019, respectively (Fig. 5A). This substantial proportion from indirect N deposition is primarily attributed to the total river area (approximately 10^3 km^2) across the 33 sub-basins being much smaller than the land area (approximately 3.8×10^6 km^2). A previous study reported a total direct N deposition of 237 kton $year^{-1}$ to inland waters of China during the 2010s, resulting in an average increase in riverine N concentrations of 64 g m^{-3} $year^{-1}$ (*15*). While our findings regarding directly deposited N inputs to rivers (2011: 289 kton; 2019: 311 kton) align with this earlier study, the contribution of N deposition to the N concentrations in rivers is much higher if indirect N deposition is included. These elevated N inputs substantially increase the total N/total phosphorus (P) ratio (*39*, *40*) and trigger eutrophication in inland water bodies (*41*).

The N inputs to rivers from both direct and indirect N deposition from human activities increased by 3% averaged over the 33 sub-basins in the 2010s (based on the ST1 experiment; Fig. 5B). However, this spatially averaged decrease masks substantial geographical variations. While N inputs from total (direct and indirect) N deposition increased by between 2 and 14% between 2011 and 2019 for the most of the southern river basins (Yangtze, Pearl, Menjiang, Hanjiang, and Jiulong), in all northern river basins (Fuchun and Oujiang), N inputs to rivers from N deposition decreased by 1 to 17%. This is attributed to the decrease of NO_y deposition in the northern sub-basins and the increase of NH_x deposition in the southern sub-basins from human activities, as illustrated in fig. S8. These findings suggest that N deposition impacts on water pollution were highly dependent on regional NO_x and NH_3 emission control policies. On the basis of these findings, we assessed the potential impacts of N deposition from human activities on water pollution in 2050, according to the results of ST3 scenario (Fig. 5C). With the implementation of acid emissions control alongside stringent regulation of agricultural NH_3 emissions (table S3), N inputs to rivers from total N deposition are expected to decrease by an average of 47% across all river basins in 2050 compared to 2019. Particularly noteworthy is the reduction of more than 50% in the southern river basins, except for the Jiulong sub-basin (which is projected to decrease by 48%). The results provide compelling evidence of the notable positive impact of the coordinated implementation of acid emissions and

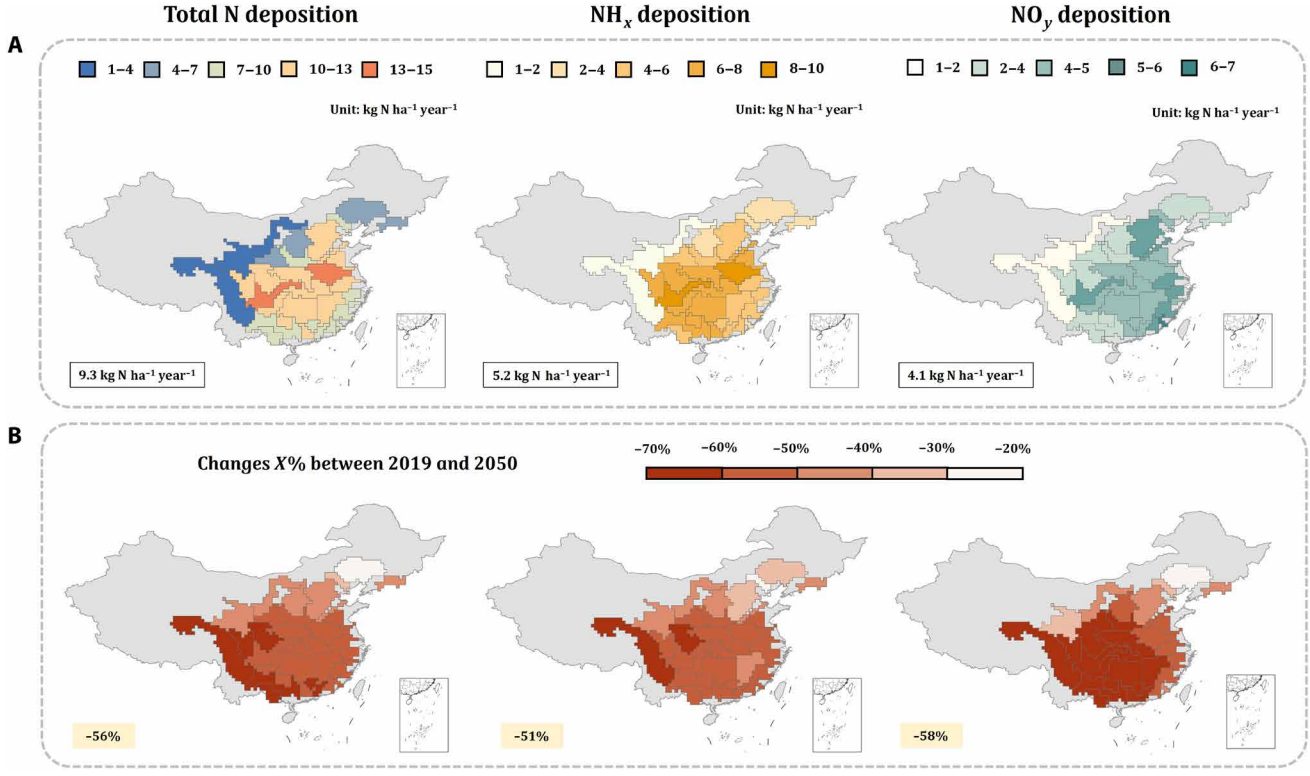

Fig. 4. Future N deposition and projected changes between 2019 and 2050. (**A**) Modeled total N, reduced N (NH_x), and oxidized N (NO_y) deposition to land only from human activities in 33 Chinese sub-basins for 2050 using GEOS-Chem at 0.5° × 0.625° horizontal resolution (ST3). The boxed numbers are the average total N, NH_x, and NO_y deposition to land across all 33 sub-basins. (**B**) Changes in total N, NH_x, and NO_y deposition only from human activities between 2019 (table S2) and 2050. The numbers in the boxes are the average changes of total N, NH_x, and NO_y deposition across all sub-basins.

agricultural NH_3 emission control measures in mitigating the effects of N deposition on water pollution in the future. As a result, if there is a 50% reduction in N deposition inputs by 2050 compared to 2012, coupled with enhancements in nutrient use efficiencies within the agricultural sector (such as implementing balanced fertilization practices for crop production and refining management strategies for animal production), then the inputs of DIN into rivers are forecasted to decrease by 64% compared to the baseline scenario of SSP5-8.5 (*41*). These findings emphasize the critical importance of embracing a comprehensive approach that takes into account the interplay between water and air quality dynamics from N deposition.

The inclusion of meteorological changes between 2011 and 2019 revealed distinct differences in the changes of N inputs to rivers from N deposition across various sub-basins, as compared to changes solely attributed to anthropogenic activities (shown by the numbers in Fig. 5, A and B). These disparities primarily stem from the influence on N deposition of differences in meteorological conditions between these 2 years. Precipitation is a crucial meteorological influence on wet N deposition (*27*). Notably, we found a notably greater difference in average precipitation rate between 2011 and 2019 in the southern sub-basins (0.2 g m^{-2} s^{-1}) compared to the northern sub-basins (0.03 g m^{-2} s^{-1}) (fig. S7). Consequently, the average wet N deposition exhibited a notable increase of 4 kg N ha^{-1} $year^{-1}$ in all southern sub-basins, in contrast to a decrease of 1 kg N ha^{-1} $year^{-1}$ in the northern sub-basins (fig. S15). These discrepancies further resulted in a substantially higher increase in N inputs to rivers from N deposition in southern river basins (such as the Yangtze, Pearl, Fuchun, and Oujiang river basins) in 2019 (Fig. 5A). As climate change–induced precipitation changes may also considerably increase riverine total N loading (*11*), it is essential for water quality management strategies in China to take account of this factor as well.

Implications

This study coupled atmospheric chemistry and water quality models to assess the effectiveness of atmospheric emissions policies in mitigating the impact of N deposition on water pollution in China. Our integrated air-water method is the first to assess the impacts of all N deposition on water quality. Our findings reveal that acid gas emission control policies did not effectively reduce N deposition to land and therefore that the associated water pollution from N deposition also did not reduce during the last decade. The 33 Chinese sub-basins investigated experienced a substantial increase of 55% in total N deposition between 1991 and 2019. Removing the effects of different annual meteorology showed that, despite the implementation of emission controls in China, human activities caused the total N deposition to increase by 18.3% in the 1990s, decrease by 2.7% in the 2000s, and increase by 0.5% in the 2010s. Especially in the 2010s, NH_x deposition increased because of the increased agricultural contribution to total N deposition (30% contribution in 2011 and 37% in 2019). Consequently, N inputs to rivers via both direct and indirect deposition increased by 3% between 2011 and 2019, with indirect N deposition as the main contributor (77 to 99% of the N inputs to rivers from N deposition).

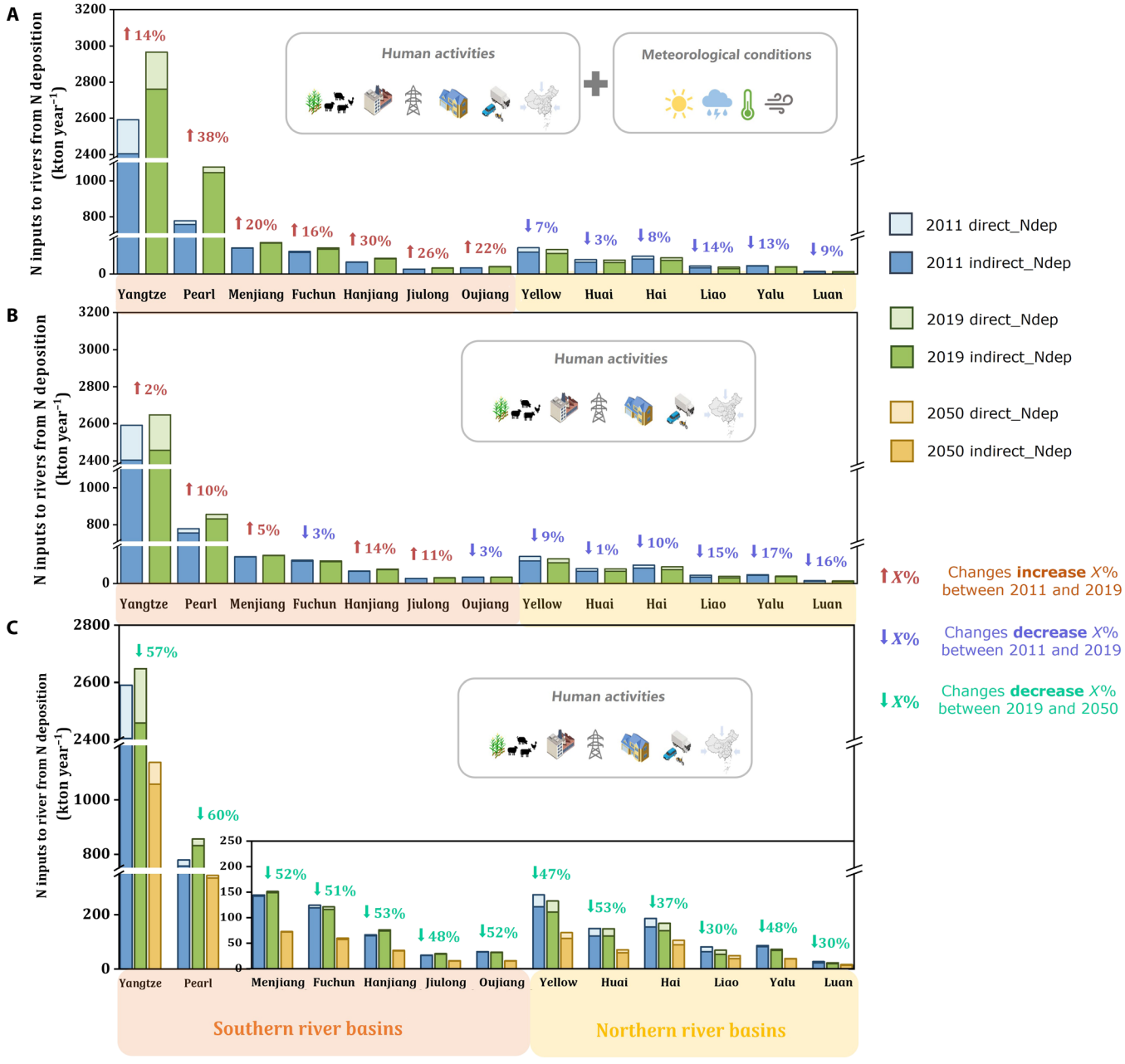

Fig. 5. N inputs to rivers from direct and indirect deposition across various research years. (**A**) N inputs to rivers from direct and indirect N deposition in simulations including both human activities and meteorological conditions in 2011 and 2019. (**B**) N inputs to rivers from direct and indirect N deposition considering human activities only (ST1 in Materials and Methods) in 2011 and 2019. (**C**) N inputs to rivers from direct and indirect N deposition considering human activities only (ST1 and ST3 in Materials and Methods) in 2011, 2019, and 2050. The columns with light colours, direct_N_{dep}, represent N deposition to water via the direct path (N deposition to open water bodies directly); the columns with dark colors, indirect_N_{dep}, represent N deposition in water via the indirect path (N deposition via transfer from soils to rivers). The arrows and percentage values above the columns in (A) and (B) indicate the changes in N inputs to each river from total N deposition (direct and indirect) between 2011 and 2019. The arrows and percentage values above the columns in (C) indicate the changes in N inputs to each river from total N deposition (direct and indirect) between 2019 and 2050. Direct N deposition was simulated by the GEOS-Chem model, and indirect N deposition was simulated by coupling the GEOS-Chem and MARINA-Nutrients models (fig. S2).

Ensuring access to clean water is vital to achieving UN SDGs (*42*), but human activities are putting enormous pressure on freshwater systems (*43*). Current policies on water quality in China focus on controlling sources directly adding aqueous pollution to rivers, such as industry and agricultural run-off. Our findings reveal that atmospheric N deposition is an important source of water pollution, especially for the overlooked indirect N deposition from the atmosphere to the watershed land (average contribution >90% in the 2010s) in previous studies. Hence, it is crucial to consider both direct and indirect N deposition to water bodies when quantifying and managing water pollution in individual sub-basins. Emission controls in areas with high N deposition levels, such as the southern

sub-basins (fig. S1), should be more stringent, while more moderate controls may be appropriate in areas with lower N deposition levels, such as Jinsha, Lanzhou, and Toudaoguai sub-basins. This approach could support the formulation of effective control of N deposition while minimizing the impact on regional economic development.

We found that agriculture was the dominant contributor to total N deposition in the 33 sub-basins in the 2010s (2011 and 2019). Despite the implementation of air pollution control policies since the 2010s, the estimated increases in NH_x deposition in our model simulations suggested that current efforts are insufficient to reduce N deposition and its impact on water pollution effectively. Reducing NH_3 emissions from agricultural sources should be a priority to reduce N deposition in the sub-basins. Our future scenario simulation confirms that coordinating acid and agricultural NH_3 emission controls is projected to decrease total N deposition and its inputs to water by 56 and 47%, respectively, by 2050 compared to the levels observed in the 2010s. Areas with high NH_x deposition areas, especially in most southern sub-basins, show notable potential for reducing the impact of N deposition on water N inputs (expected to decrease by more than 50% in 2050). While future scenarios account for controls such as intensified cultivation, grazing management enhancements, and the promotion of slow-release fertilizer, further reductions in NH_x deposition can be achieved by improving animal manure and management practices, such as using manure surface covers, injection, and rapid manure drying. Furthermore, it is also important to identify the contributions of different types of animals and crops to N deposition from agricultural sources. This will contribute to providing precision management for crop and animal production. Agricultural activities played a crucial role in water pollution, exploring synergistic measures involving water and air should be a priority, as this will help simultaneously reduce N deposition and water pollution.

MATERIALS AND METHODS

Study area

We quantified the N deposition to 13 Chinese river basins, which collectively drain 40% (approximately 4 million km^2) of China's land area (fig. S1). To facilitate a better understanding of the spatial variations in human activities within the three largest river basins, the Yellow, Yangtze, and Pearl River drainage basins were divided into 6, 11, and 6 sub-basins, respectively (*14*), yielding a study domain of 33 sub-basins in total. The other 10 river basins comprise the Huai, Hai, Luan, Liao, Yalu, Fuchun, Oujiang, Menjiang, Jiulong, and Hanjiang Rivers. All sub-basins were further classified as southern or northern (table S4).

Estimating atmospheric N deposition and its response to anthropogenic emission changes

We used the GEOS-Chem v12.9.3 (http://geos-chem.org) three-dimensional global CTM to simulate N deposition over the 33 Chinese sub-basins for six target years (1991, 1999, 2001, 2009, 2011, and 2019) in three decades (1990s, 2000s, and 2010s). The selected target years did not include any extreme weather conditions so as to focus attention on the impacts of the implemented emissions policies on N deposition across the decades. The target years also allow assessment of any lag effect of policies on N deposition. The CTM is driven using MERRA-2 assimilated meteorological data from the Global Modeling and Assimilation Office (GMAO) of the National Aeronautics and Space Administration (NASA). The meteorological fields of temperature, relative and specific humidity, vertical pressure velocity, and surface pressure have a temporal resolution of 3 hours, while sea-level pressure, tropopause pressure, and other surface variables have a temporal resolution of 1 hour. The model has 47 vertical layers from the surface to 0.01 hPa, and the midpoint of the lowest layer is 58 meter above sea level (*44*). In this study, we used a nested version of GEOS-Chem with a horizontal resolution of 0.5° × 0.625° over China and 4° × 5° for the rest of the world. All simulations were initiated after a half-year spin-up.

The model provides detailed simulations of tropospheric ozone-NO_x-hydrocarbon-aerosol chemistry (*45*, *46*). Gas and aerosol-phase chemistry are coupled through heterogeneous aerosol chemistry that is parameterized as reactive uptake coefficients (*47*), aerosol effects on photolysis rates (*48*), and gas-aerosol partitioning of total NH_3 and HNO_3 using the ISORROPIA II thermodynamic equilibrium model (*49*). Dry deposition fluxes are calculated by multiplying the concentration in the lowest model layer with the dry deposition velocity, which is parameterized using the standard resistance-in-series model (*50*, *51*). The dry deposition flux out of the lowest model layer is calculated as

$$Fd = n_a C(z1) vd(z1)$$

Fd is dry deposition flux, n_a (molecules cm^{-3}) is the number density of air, $C(z1)$ is the mixing ratio of the deposition species at height $z1$, and vd is the dry deposition velocity (cm s^{-1}) at the specific height.

The deposition velocity is a function of the local meteorological condition and surface type

$$V_d = \frac{1}{R_a(Z_1, Z_0) + R_b + R_c}$$

Here, R_a (Z_1, Z_0) is the aerodynamic resistance to turbulent transfer from Z_1 to the roughness height Z_0 close to the surface where turbulence vanishes, R_b is the boundary layer resistance to molecular diffusion from Z_0 to the actual surface, and R_c is the canopy or surface uptake resistance (*21*). The land use types include urban land, agricultural land, range land, deciduous forest, coniferous forest, mixed forest including wetland, water (both salt and fresh), barren land (mostly desert), nonforested wetland, mixed agricultural and range land, and rocky open areas with low-growing shrubs. Wet deposition fluxes are estimated through the parameterization of in-cloud and subcloud clearance processes caused by large-scale precipitation and convective updrafts.

Emissions in the GEOS-Chem model were processed using HEMCO (Harvard-NASA Emission Component) (*52*). Anthropogenic emissions of SO_2, carbon monoxide (CO), NO_x, and NH_3 in 2009, 2011, and 2019 over China were obtained from the Multi-resolution Emission Inventory for China (MEIC; http://meicmodel.org) (*34*, *53*). Anthropogenic emissions in 1991, 1999, and 2001 over China were processed using the Community Emissions Data System (CEDS) according to the annual ratio of the grid in the MEIC inventory. The CEDS is a global dataset including annual historical anthropogenic reactive gases like CO, CH_4, NH_3, NO_x, SO_2, and NMVOCs from 1750 to 2014. The CEDS emission inventory reports annual country-total emissions from six main sectors (energy production, industry, transportation, agriculture, waste, and RCO ("residential, commercial, and other") (*54*). Emissions over Asia used the MIX inventory (www.meicmodel.org/dataset-mix) (*55*), with those for China overwritten by the MEIC inventory. Natural

emissions of NO_x from biomass burning, soil, and lighting were also included.

In ST1, three additional model sensitivity tests were conducted to explore variations in N deposition caused only by human activities in each decade (the 1990s: ST1-1990s, the 2000s: ST1-2000s, and the 2010s: ST1-2010s). The ST1 simulations used the anthropogenic emission inventory relevant to the given year but with 1991, 2001, or 2011 fixed meteorology; for example, the ST1 simulations for the 1990s used 1991 and 1999 anthropogenic emissions but only 1991 meteorology. This allowed our analysis to focus solely on the responses of N deposition to changes in anthropogenic emissions caused by emission control policies in each decade while also allowing for the lag effects of the policies, the effects of China's phased tasks in atmospheric emission policies over each decade (after two 5-year plan), and consistency with the years of actual N deposition simulations.

In ST2, simulations were conducted to assess the contributions to N deposition in the 2010s from the following emission sectors: agriculture, industry, power plants, residential, transportation, and others (includes international transport, soil, lightning, and biomass burning). The individual contribution of each emission source to N deposition was determined from the difference between simulations from ST1-2010s with a sector source turned off and one that included all emissions. These model experiments have been described in detail previously (*20*, *22*).

In ST3: The model simulations were conducted to assess the N deposition in 2050. The ST3 simulations used the anthropogenic emission inventory of SSP5-85–best health effect (BHE) from Tong *et al.* (*38*) but with fixed meteorology from 2011. Tong *et al.* (*38*) developed a dynamic projection model (the Dynamic Projection model for Emissions in China) to explore China's future anthropogenic emission pathways and then connected a series of SSP, representative concentration pathway (RCP), and pollution control scenarios to present a wide range of China's future emissions to 2050 under different development and policy pathways. Specifically, we chose the socioeconomic pathway 5 (SSP5)–85–BHE scenario in our study to simulate N deposition as it represents high pollution control ambitions for 2050. It combines the shared SSP5 with climate forcing outcomes as described by the RCP 8.5. This scenario represents integrated global societies with low population growth, high consumption of fossil fuels, highly managed environmental conditions at local scales, and the highest greenhouse gas concentrations for climate change (RCP8.5). The BHE component ensures a clean environment and maximum protection of public health. It requires the application of the best-available technology to eventually achieve the World Health Organization Interim Target 3 of 15 $\mu g\ m^{-3}$ annual mean $PM_{2.5}$ by 2050. Under the accompanying global development trend, the manufacture and end-of-pipe control technologies in China would gradually catch up with developed countries. The BHE controls for different sectors are shown in table S3, and the corresponding predicted anthropogenic emissions of SO_2, NO_x, and NH_3 in China are shown in fig. S14.

Quantification of impacts of N deposition on water pollution

We used the MARINA-Nutrients (version 2.0) model to quantify the N inputs to rivers from indirect N deposition. The model was developed to quantify the annual river export at the sub-basin scale of total dissolved N (TDN) and total dissolved P from different sources (*14*). TDN is the sum of DIN and dissolved organic N. The model quantifies the export of nutrients to seas in three steps. First, nutrient inputs into rivers from diffuse and point sources are quantified. Second, nutrient exports to the outlet of each sub-basin are quantified in which nutrient retentions (e.g., sedimentation, damming) and losses (e.g., denitrification and water consumption) are taken into account. Third, exports of nutrients from sub-basin outlets to river mouths are quantified (*7*). MARINA-Nutrients model therefore accounts for many factors influencing nutrient flow from Chinese rivers into Chinese seas, including human activities on land, basin hydrological characteristics, retention and loss of nutrients in soils and rivers, and distances that nutrients travel to the river mouth. In this study, we used the first step in the model for quantifying N input to rivers from indirect N deposition on land. A detailed description of MARINA-Nutrients (version 2.0) is provided in the text S1 and fig. S16.

We quantified the direct deposition of N to open water bodies of the sub-basins (direct path) and the transportation of N deposition on agricultural and nonagricultural land to surface waters (indirect path) in the 2010s (years 2011 and 2019) and projected for 2050. The quantification steps are outlined as follows:

(i) The direct N deposition is calculated in two steps. First, the total N deposition on the sub-basin's surface including both land and water was determined by multiplying the average N deposition intensity per unit area in each grid (kg N ha^{-1} $year^{-1}$) by the grid area (ha) and then aggregating these values at the sub-basin scale (fig. S17). Second, the direct N deposition for each sub-basin in our study was calculated by multiplying the total N deposition on the sub-basin's surface by the share of surface water area to total sub-basin area (kton N $year^{-1}$).

(ii) For N deposition via the indirect path, we used the MARINA-Nutrients (version 2.0) model to quantify the N inputs to rivers from indirect N deposition. We first need to adjust the resolution from the CTM to match the scale of the MARINA-Nutrients model (at the sub-basin level). In detail, first, the GEOS-Chem model simulated N deposition across the entirety of China using a grid resolution of 0.5° latitude by 0.625° longitude (unit: kton N). This resolution is converted to 0.5° latitude by 0.5° longitude grids within ArcGIS (Resample Function). This adjustment is necessary because the sub-basin division is on a 30-arcmin grid scale (equivalent to 0.5° × 0.5°) as it is based on a global drainage direction map at this resolution (*56*). The smallest area of sub-basins in this study (named Jiulong and Oujiang) encompasses six grids of 0.5° × 0.5°. Second, the gridded N deposition data on land were aggregated to sub-basin levels by summing the values of the grids that fall within each sub-basin boundary. This aggregation process was performed using the "zonal statistics" function in ArcGIS. Further detail of resolution conversion is provided in fig S17. Third, the N deposition data at the sub-basin scale serves as the input for the MARINA-Nutrients model, enabling the calculation of indirect N deposition in our study via the following equations (*7*, *14*)

$$RSdif_{\mathrm{DIN.dep.ant.j}} = WSdif_{\mathrm{N.dep.ant.j}} \cdot FE_{\mathrm{WS.DIN.j}} \cdot G_{\mathrm{DIN.j}} \quad (1)$$

$$RSdif_{\mathrm{DIN.dep.nat.j}} = WSdif_{\mathrm{N.dep.nat.j}} \cdot FE_{\mathrm{WS.DIN.j}} \quad (2)$$

$$G_{\mathrm{DIN.j}} = 1 - \left(WSdif_{\mathrm{N.ex.j}} / WSdif_{\mathrm{N.gross.j}} \right) \quad (3)$$

$$FE_{\mathrm{WS.DIN.j}} = Rnat_{\mathrm{j}} \cdot eF \quad (4)$$

$$Rnat_{\mathrm{j}} = Qnat_{\mathrm{j}}/Area_{\mathrm{j}} \quad (5)$$

Here, $RSdif_{\mathrm{DIN.dep.ant.j}}$ and $RSdif_{\mathrm{DIN.dep.nat.j}}$ are inputs (kg year^{-1}) of dissolved inorganic nitrogen (DIN) to surface waters in sub-basin *j* from atmospheric N deposition to agricultural and non-agricultural areas, respectively. $WSdif_{\mathrm{N.dep.ant.j}}$ and $WSdif_{\mathrm{N.dep.nat.j}}$ are the atmospheric N depositions (kg year^{-1}) in sub-basin *j* to agricultural and nonagricultural areas, respectively. $FE_{\mathrm{WS.DIN.j}}$ is the export fraction of DIN entering surface waters of sub-basin *j*; the fraction is calculated as a function of annual runoff from land to streams. The parameters of $FE_{\mathrm{WS.DIN.j}}$ in each sub-basin are shown in table S4. $G_{\mathrm{DIN.j}}$ is the fraction of DIN applied to agricultural land that remained in the soils of sub-basin *j* after animal grazing and crop harvesting. $WSdif_{\mathrm{N.ex.j}}$ is the export of nutrient elements from agricultural areas by animal grazing and crop harvesting (kg year^{-1}). $WSdif_{\mathrm{N.gross.j}}$ is the total input of N to agricultural soils from diffuse sources, including the use of animal manure, synthetic fertilizer and human excretion in agriculture, atmospheric N deposition to agricultural areas, and biological N_2 fixation by agricultural crops (kg year^{-1}).

Aside from the atmospheric N deposition source, the other sources of N inputs (synthetic fertilizers, animal manure, human waste, and biological N_2 fixation) to land in 2011 were taken from Wang *et al.* (*57*), which were aggregated from counties in China to 0.5° × 0.5° grids and sub-basins using ArcGIS in Wang *et al.* (*14*). On the basis of the previous study of the N budget in China by Zhang *et al.* (*58*), the nitrogen use efficiency of croplands in the 2010s was kept constant; thus, we assumed that $G_{\mathrm{DIN.j}}$ was the same in 2011 and 2019. For the year 2050, we used the scenario (SSP5-RCP8.5) of other sources developed by Wang *et al.* (*14*). The SSP5 scenario assumes integrated global societies with low population growth, high consumption of fossil fuels, and highly managed environmental conditions at local scales. RCP8.5 means the highest greenhouse gas concentrations for climate change.

eF is the watershed (land) export constant, which is 0.94 for DIN; this parameter is derived from the original Global Nutrient Export from WaterSheds 2 (NEWS 2) model by Mayorga *et al.* and Strokal et al. (*7*, *59*). $Rnat_j$ is the annual runoff from land to streams in sub-basin *j* (m). $Qnat_j$ is the natural river discharge at the outlet of sub-basin *j* before water is removed for consumption (km^3 year^{-1} km^2); this model input was aggregated from a spatial resolution of 0.5° × 0.5° to sub-basins for Chinese rivers using the approach described in Strokal *et al.* (*7*). We used the water discharge values from five variable infiltration capacity model runs with climate inputs (e.g., precipitation and temperature) from different general climate models (GCMs): GFDL-ESM2M, HadGEM2-ES, IPSL-CM5A-LR, MIROC5-ESM-CHEM, and NORESM1-M (*60*). Average water discharge values from these five runs were used to harmonize the uncertainties introduced by the GCMs. We used the ensemble-average (30-year average) annual water discharge for 2011 and 2019, so that our result was less affected by modelled discharge extremes. For example, the annual water discharge values from 1996 to 2026 were averaged to derive the water discharge in 2011. The specific $Qnat_j$ values over the 33 sub-basins in 2011, 2019, and 2050 are shown in fig. S18. $Area_j$ is the drainage area of sub-basin *j* (km^2) (table S4).

Observation data

GEOS-Chem model simulations of N deposition over China have been evaluated in previous studies (*20*, *61*). We further evaluated our GEOS-Chem simulations using available observations for China. The annual mean NH_4^+ and NO_3^- wet deposition were compared with data from the Acid Deposition Monitoring Network in East Asia (EANET; www.eanet.asia/event-and-activities), the study of Liu *et al.* (*1*) and the Nationwide Nitrogen Deposition Monitoring Network (NNDMN) (*23*, *62*, *63*) from 1991 to 2011. Owing to practical difficulties in obtaining observational dry deposition fluxes, these were usually estimated using measured surface concentrations and modelled dry deposition velocities (*44*, *62*, *64*). Therefore, we compared the modeled surface NH_3 concentrations with the available NNDMN observations for 2011. Details of the years and numbers of measurement locations used for model evaluation for each dataset are shown in table S5. For 2019, the simulation of the annual mean NH_4^+ and NO_3^- wet deposition and surface NH_3 concentrations was compared with measurements at 49 sites across China (fig. S19). Details of sampling and analysis are provided in text S2.

To determine the SO_2 and NO_2 annual trends in China, we obtained real-time data at 1498 monitoring sites including 367 cities during 2015–2019 from the China National Environmental Monitoring Centre (www.cnemc.cn/). The distribution of monitoring sites and annual mean observed concentrations of SO_2 and NO_x are shown in fig. S11.

Model evaluation

We evaluated the GEOS-Chem model simulation of N deposition over China using surface measurements available over the three decades of NH_4^+ and NO_3^- wet deposition fluxes and NH_3 gas concentration. As shown in fig. S20, correlation coefficients (*r*) between model simulations and observations for wet deposition were greater than 0.5, and normalized mean biases (NMBs) were less than 13%. The modeled surface NH_3 concentrations reproduced the observed NH_3 concentrations with *r* greater than 0.6 and NMB within 30%. On the basis of previous studies (*45*), the model could generally reproduce the observed spatial and temporal variations in wet Nr deposition and NH_3 concentrations.

To evaluate the direct N deposition results, we compared our findings with other studies focused on the same sub-basins. Detailed results are provided in text S3.

The MARINA-Nutrients model (version 2.0) was evaluated by Wang *et al.* (*14*). They applied three options that so-called "building trust" approach, including model validation by comparing the modeled loads of nutrients with measurements, comparing results from other modelled studies and performing a sensitivity analysis. The validation provides confidence in using the modeling approaches for China in our analyses. Moreover, despite the updating of N deposition data for each sub-basin in our study, when as the input of the MARINA-Nutrients model, the simulated TDN and DIN export across 12 river basins remain consistent with both measurement and modeling studies. Further details regarding the MARINA-Nutrients model validation are described in text S4.

Supplementary Materials

The PDF file includes:

Supplementary Texts S1 to S4
Figs. S1 to S21
Tables S1 to S6
Legends for data S1 to S4
References

Other Supplementary Material for this manuscript includes the following:

Data S1 to S4

REFERENCES AND NOTES

1. X. Liu, Y. Zhang, W. Han, A. Tang, J. Shen, Z. Cui, P. Vitousek, J. W. Erisman, K. Goulding, P. Christie, A. Fangmeier, F. Zhang, Enhanced nitrogen deposition over China. *Nature* **494**, 459–462 (2013).
2. X. Huang, Y. Song, M. Li, J. Li, Q. Huo, X. Cai, T. Zhu, M. Hu, H. Zhang, A high-resolution ammonia emission inventory in China. *Global Biogeochem. Cycles* **26**, GB1030 (2012).
3. D. Fowler, M. Coyle, U. Skiba, M. A. Sutton, J. N. Cape, S. Reis, L. J. Sheppard, A. Jenkins, B. Grizzetti, J. N. Galloway, P. Vitousek, A. Leach, A. F. Bouwman, K. Butterbach-Bahl, F. Dentener, D. Stevenson, M. Amann, M. Voss, The global nitrogen cycle in the twenty-first century. *Philosop. Transact. R. Soc B: Biol. Sci.* **368**, 20130164 (2013).
4. J. N. Galloway, F. J. Dentener, D. G. Capone, E. W. Boyer, R. W. Howarth, S. P. Seitzinger, G. P. Asner, C. C. Cleveland, P. A. Green, E. Holland, D. M. Karl, A. F. Michaels, J. H. Porter, A. R. Townsend, C. J. Vöosmarty, Nitrogen cycles: Past, present, and future. *Biogeochemistry* **70**, 153–226 (2004).
5. W. H. Schlesinger, On the fate of anthropogenic nitrogen. *Proc. Natl. Acad. Sci. U.S.A.* **106**, 203–208 (2009).
6. J. Johnson, E. Graf Pannatier, S. Carnicelli, G. Cecchini, N. Clarke, N. Cools, K. Hansen, H. Meesenburg, T. M. Nieminen, G. Pihl-Karlsson, H. Titeux, E. Vanguelova, A. Verstraeten, L. Vesterdal, P. Waldner, M. Jonard, The response of soil solution chemistry in European forests to decreasing acid deposition. *Glob. Chang. Biol.* **24**, 3603–3619 (2018).
7. M. Strokal, C. Kroeze, M. Wang, Z. Bai, L. Ma, The MARINA model (Model to Assess River Inputs of Nutrients to seAs): Model description and results for China. *Sci. Total Environ.* **562**, 869–888 (2016).
8. J. Wang, A. H. W. Beusen, X. Liu, R. Van Dingenen, F. Dentener, Q. Yao, B. Xu, X. Ran, Z. Yu, A. F. Bouwman, Spatially explicit inventory of sources of nitrogen inputs to the Yellow Sea, East China Sea, and South China Sea for the period 1970–2010. *Earth's Future* **8**, e2020EF001516 (2020).
9. X. Zhan, Y. Bo, F. Zhou, X. Liu, H. W. Paerl, J. Shen, R. Wang, F. Li, S. Tao, Y. Dong, X. Tang, Evidence for the importance of atmospheric nitrogen deposition to eutrophic Lake Dianchi, China. *Environ. Sci. Technol.* **51**, 6699–6708 (2017).
10. G. Midolo, R. Alkemade, A. M. Schipper, A. Benítez-López, M. P. Perring, W. De Vries, X. Xu, Impacts of nitrogen addition on plant species richness and abundance: A global meta-analysis. *Glob. Ecol. Biogeogr.* **28**, 398–413 (2018).
11. E. Sinha, A. M. Michalak, V. Balaji, Eutrophication will increase during the 21st century as a result of precipitation changes. *Science* **357**, 405–408 (2017).
12. M. Strokal, J. E. Spanier, C. Kroeze, A. A. Koelmans, M. Flörke, W. Franssen, N. Hofstra, S. Langan, T. Tang, M. T. H. van Vliet, Y. Wada, M. Wang, J. van Wijnen, R. Williams, Global multi-pollutant modelling of water quality: scientific challenges and future directions. *Curr. Opin. Environ. Sustain.* **36**, 116–125 (2019).
13. United Nations, *Transforming our world: the 2030 agenda for sustainable development* (United Nations, New York, 2015); https://sdgs.un.org/2030agenda.
14. M. Wang, C. Kroeze, M. Strokal, M. T. H. Vliet, L. Ma, Global change can make coastal eutrophication control in China more difficult. *Earth's Future* **8**, e2019EF001280 (2020).
15. Y. Gao, F. Zhou, P. Ciais, C. Miao, T. Yang, Y. Jia, X. Zhou, B. B. Klaus, T. Yang, G. Yu, Human activities aggravate nitrogen-deposition pollution to inland water over China. *Natl. Sci. Rev.* **7**, 430–440 (2020).
16. X. Chen, M. Strokal, M. T. H. Van Vliet, J. Stuiver, M. Wang, Z. Bai, L. Ma, C. Kroeze, Multi-scale modeling of nutrient pollution in the rivers of China. *Environ. Sci. Technol.* **53**, 9614–9625 (2019).
17. R. A. Bellmore, J. E. Compton, J. R. Brooks, E. W. Fox, R. A. Hill, D. J. Sobota, D. J. Thornbrugh, M. H. Weber, Nitrogen inputs drive nitrogen concentrations in U.S. streams and rivers during summer low flow conditions. *Sci. Total Environ.* **639**, 1349–1359 (2018).
18. S. Chen, L. Chen, X. Liu, Y. Pan, F. Zhou, J. Guo, T. Huang, F. Chen, Z. Shen, Unexpected nitrogen flow and water quality change due to varying atmospheric deposition. *J. Hydrol.* **609**, 127679 (2022).
19. L. Liu, W. Xu, X. Lu, B. Zhong, Y. Guo, X. Lu, Y. Zhao, W. He, S. Wang, X. Zhang, X. Liu, P. Vitousek, Exploring global changes in agricultural ammonia emissions and their contribution to nitrogen deposition since 1980. *Proc. Natl. Acad. Sci. U.S.A.* **119**, e2121998119 (2022).
20. Y. Zhao, L. Zhang, Y. Chen, X. Liu, W. Xu, Y. Pan, L. Duan, Atmospheric nitrogen deposition to China: A model analysis on nitrogen budget and critical load exceedance. *Atmos. Environ.* **153**, 32–40 (2017).
21. L. Zhang, D. J. Jacob, E. M. Knipping, N. Kumar, J. W. Munger, C. C. Carouge, A. van Donkelaar, Y. X. Wang, D. Chen, Nitrogen deposition to the United States: Distribution, sources, and processes. *Atmosp. Chem. Phys.* **12**, 4539–4554 (2012).
22. W. Xu, Y. Zhao, X. Liu, A. J. Dore, L. Zhang, L. Liu, M. Cheng, Atmospheric nitrogen deposition in the Yangtze River basin: Spatial pattern and source attribution. *Environ. Pollut.* **232**, 546–555 (2018).
23. Z. Wen, W. Xu, Q. Li, M. Han, A. Tang, Y. Zhang, X. Luo, J. Shen, W. Wang, K. Li, Y. Pan, L. Zhang, W. Li, J. L. Collett Jr., B. Zhong, X. Wang, K. Goulding, F. Zhang, X. Liu, Changes of nitrogen deposition in China from 1980 to 2018. *Environ. Int.* **144**, 106022 (2020).
24. Z. Bai, W. Winiwarter, Z. Klimont, G. Velthof, T. Misselbrook, Z. Zhao, X. Jin, O. Oenema, C. Hu, L. Ma, Further improvement of air quality in China needs clear ammonia mitigation target. *Environ. Sci. Technol.* **53**, 10542–10544 (2019).
25. X. Zhang, B. Gu, H. van Grinsven, S. K. Lam, X. Liang, M. Bai, D. Chen, Societal benefits of halving agricultural ammonia emissions in China far exceed the abatement costs. *Nat. Commun.* **11**, 4357 (2020).
26. W. Xu, L. Liu, M. Cheng, Y. Zhao, L. Zhang, Y. Pan, X. Zhang, B. Gu, Y. Li, X. Zhang, J. Shen, L. Lu, X. Luo, Y. Zhao, Z. Feng, J. L. Collett Jr., F. Zhang, X. Liu, Spatial–temporal patterns of inorganic nitrogen air concentrations and deposition in eastern China. *Atmosp. Chem. Phys.* **18**, 10931–10954 (2018).
27. Y. Zhao, M. Xi, Q. Zhang, Z. Dong, M. Ma, K. Zhou, W. Xu, J. Xing, B. Zheng, Z. Wen, X. Liu, C. P. Nielsen, Y. Liu, Y. Pan, L. Zhang, Decline in bulk deposition of air pollutants in China lags behind reductions in emissions. *Nat. Geosci.* **15**, 190–195 (2022).
28. D. Ackerman, D. B. Millet, X. Chen, Global estimates of inorganic nitrogen deposition across Four decades. *Global Biogeochem. Cycles* **33**, 100–107 (2019).
29. G. Yu, Y. Jia, N. He, J. Zhu, Z. Chen, Q. Wang, S. Piao, X. Liu, H. He, X. Guo, Z. Wen, P. Li, G. Ding, K. Goulding, Stabilization of atmospheric nitrogen deposition in China over the past decade. *Nat. Geosci.* **12**, 424–429 (2019).
30. Z. Bai, W. Ma, L. Ma, G. L. Velthof, Z. Wei, P. Havlík, O. Oenema, M. R. F. Lee, F. Zhang, China's livestock transition: Driving forces, impacts, and consequences. *Sci. Adv.* **4**, eaar8534 (2018).
31. Y. Chen, L. Zhang, Y. Zhao, L. Zhang, J. Zhang, M. Liu, M. Zhou, B. Luo, High-Resolution ammonia emissions from nitrogen fertilizer application in China during 2005–2020. *Atmos.* **13**, GB1030 (2022).
32. D. Xu, B. Ge, Z. Wang, Y. Sun, Y. Chen, D. Ji, T. Yang, Z. Ma, N. Cheng, J. Hao, X. Yao, Below-cloud wet scavenging of soluble inorganic ions by rain in Beijing during the summer of 2014. *Environ. Pollut.* **230**, 963–973 (2017).
33. J. Chen, M. Cheng, M. Krol, W. de Vries, Q. Zhu, X. Liu, F. Zhang, W. Xu, Trends in anthropogenic ammonia emissions in China since 1980: A review of approaches and estimations. *Front. Environ. Sci.* **11**, 1133753 (2023).
34. B. Zheng, D. Tong, M. Li, F. Liu, C. Hong, G. Geng, H. Li, X. Li, L. Peng, J. Qi, L. Yan, Y. Zhang, H. Zhao, Y. Zheng, K. He, Q. Zhang, Trends in China's anthropogenic emissions since 2010 as the consequence of clean air actions. *Atmosp. Chem. Phys.* **18**, 14095–14111 (2018).
35. J. X. Warner, Z. Wei, L. L. Strow, R. R. Dickerson, J. B. Nowak, The global tropospheric ammonia distribution as seen in the 13-year AIRS measurement record. *Atmosp. Chem. Phys.* **16**, 5467–5479 (2016).
36. D. Fang, B. Chen, K. Hubacek, R. Ni, L. Chen, K. Feng, J. Lin, Clean air for some: Unintended spillover effects of regional air pollution policies. *Sci. Adv.* **5**, eaav4707 (2019).
37. W. Xu, Y. Zhao, Z. Wen, Y. Chang, Y. Pan, Y. Sun, X. Ma, Z. Sha, Z. Li, J. Kang, L. Liu, A. Tang, K. Wang, Y. Zhang, Y. Guo, L. Zhang, L. Sheng, X. Zhang, B. Gu, Y. Song, M. Van Damme, L. Clarisse, P.-F. Coheur, J. L. Collett, K. Goulding, F. Zhang, K. He, X. Liu, Increasing importance of ammonia emission abatement in PM2.5 pollution control. *Sci. Bull.* **67**, 1745–1749 (2022).
38. D. Tong, J. Cheng, Y. Liu, S. Yu, L. Yan, C. Hong, Y. Qin, H. Zhao, Y. Zheng, G. Geng, M. Li, F. Liu, Y. Zhang, B. Zheng, L. Clarke, Q. Zhang, Dynamic projection of anthropogenic emissions in China: methodology and 2015–2050 emission pathways under a range of socio-economic, climate policy, and pollution control scenarios. *Atmosp. Chem. Phys.* **20**, 5729–5757 (2020).
39. D. J. Conley, H. W. Paerl, R. W. Howarth, D. F. Boesch, S. P. Seitzinger, K. E. Havens, C. Lancelot, G. E. Likens, Controlling eutrophication: Nitrogen and phosphorus. *Science* **323**, 1014–1015 (2009).
40. O. Deng, Y. Chen, T. Lan, S. Zhang, X. Gao, W. Zhou, D. Ou, Y. Hu, L. Luo, Contribution of atmospheric N deposition to riverine N load in a forest-dominated watershed through field monitoring for three years. *Chemosphere* **266**, 128951 (2021).
41. M. Wang, A. B. G. Janssen, J. Bazin, M. Strokal, L. Ma, C. Kroeze, Accounting for interactions between Sustainable Development Goals is essential for water pollution control in China. *Nat. Commun.* **13**, 730 (2022).
42. D. Griggs, M. Stafford-Smith, O. Gaffney, J. Rockström, M. C. Öhman, P. Shyamsundar, W. Steffen, G. Glaser, N. Kanie, I. Noble, Sustainable development goals for people and planet. *Nature* **495**, 305–307 (2013).
43. C. J. Vörösmarty, P. B. McIntyre, M. O. Gessner, D. Dudgeon, A. Prusevich, P. Green, S. Glidden, S. E. Bunn, C. A. Sullivan, C. R. Liermann, P. M. Davies, Global threats to human water security and river biodiversity. *Nature* **467**, 555–561 (2010).
44. Y. Chen, L. Zhang, D. K. Henze, Y. Zhao, X. Lu, W. Winiwarter, Y. Guo, X. Liu, Z. Wen, Y. Pan, Y. Song, Interannual variation of reactive nitrogen emissions and their impacts on $PM_{2.5}$ air pollution in China during 2005–2015. *Environ. Res. Lett.* **16**, 3695 (2021).
45. J. Mao, D. J. Jacob, M. J. Evans, J. R. Olson, X. Ren, W. H. Brune, J. M. S. Clair, J. D. Crounse, K. M. Spencer, M. R. Beaver, P. O. Wennberg, M. J. Cubison, J. L. Jimenez, A. Fried, P. Weibring, J. G. Walega, S. R. Hall, A. J. Weinheimer, R. C. Cohen, G. Chen, J. H. Crawford, C. McNaughton, A. D. Clarke, L. Jaeglé, J. A. Fisher, R. M. Yantosca, P. Le Sager, C. Carouge, Chemistry of hydrogen oxide radicals (HO_x) in the Arctic troposphere in spring. *Atmos. Chem. Phys.* **10**, 5823–5838 (2010).

46. R. J. Park, Natural and transboundary pollution influences on sulfate-nitrate-ammonium aerosols in the United States: Implications for policy. *J. Geophys. Res.* **109**, D15204 (2004).
47. D. J. Jacob, Heterogeneous chemistry and tropospheric ozone. *Atmos. Environ.* **34**, 2131–2159 (2000).
48. R. V. Martin, D. J. Jacob, R. M. Yantosca, M. Chin, P. Ginoux, Global and regional decreases in tropospheric oxidants from photochemical effects of aerosols. *J. Geophys. Res. Atmos.* **108**, 4097 (2003).
49. C. Fountoukis, A. Nenes, ISORROPIA II: a computationally efficient thermodynamic equilibrium model for K^+–Ca^{2+}–Mg^{2+}–NH_4^+–Na^+–SO_4^{2-}–NO_3^-–Cl^-–H_2O aerosols. *Atmos. Chem. Phys.* **7**, 4639–4659 (2007).
50. M. L. Wesely, Parameterization of surface resistances to gaseous dry deposition in regional-scale numerical models. *Atmos. Environ. (1967)* **23**, 1293–1304 (1989).
51. L. Zhang, S. Gong, J. Padro, L. Barrie, A size-segregated particle dry deposition scheme for an atmospheric aerosol module. *Atmos. Environ.* **35**, 549–560 (2001).
52. C. A. Keller, M. S. Long, R. M. Yantosca, A. M. Da Silva, S. Pawson, D. J. Jacob, HEMCO v1.0: A versatile, ESMF-compliant component for calculating emissions in atmospheric models. *Geosci. Model Dev.* **7**, 1409–1417 (2014).
53. M. Li, H. Liu, G. Geng, C. Hong, F. Liu, Y. Song, D. Tong, B. Zheng, H. Cui, H. Man, Q. Zhang, K. He, Anthropogenic emission inventories in China: a review. *Natl. Sci. Rev.* **4**, 834–866 (2017).
54. R. M. Hoesly, S. J. Smith, L. Feng, Z. Klimont, G. Janssens-Maenhout, T. Pitkanen, J. J. Seibert, L. Vu, R. J. Andres, R. M. Bolt, T. C. Bond, L. Dawidowski, N. Kholod, J.-I. Kurokawa, M. Li, L. Liu, Z. Lu, M. C. P. Moura, P. R. O'Rourke, Q. Zhang, Historical (1750–2014) anthropogenic emissions of reactive gases and aerosols from the Community Emissions Data System (CEDS). *Geosci. Model Dev.* **11**, 369–408 (2018).
55. M. Li, Q. Zhang, J. I. Kurokawa, J. H. Woo, K. He, Z. Lu, T. Ohara, Y. Song, D. G. Streets, G. R. Carmichael, Y. Cheng, C. Hong, H. Huo, X. Jiang, S. Kang, F. Liu, H. Su, B. Zheng, MIX: A mosaic Asian anthropogenic emission inventory under the international collaboration framework of the MICS-Asia and HTAP. *Atmos. Chem. Phys.* **17**, 935–963 (2017).
56. P. Döll, B. Lehner, Validation of a new global 30-min drainage direction map. *J. Hydrol.* **258**, 214–231 (2002).
57. M. Wang, L. Ma, M. Strokal, W. Ma, X. Liu, C. Kroeze, Hotspots for nitrogen and phosphorus losses from food production in China: A county-scale analysis. *Environ. Sci. Technol.* **52**, 5782–5791 (2018).
58. X. Zhang, C. Ren, B. Gu, D. Chen, Uncertainty of nitrogen budget in China. *Environ. Pollut.* **286**, 117216 (2021).
59. E. Mayorga, S. P. Seitzinger, J. A. Harrison, E. Dumont, A. H. W. Beusen, A. F. Bouwman, B. M. Fekete, C. Kroeze, G. Van Drecht, Global Nutrient Export from WaterSheds 2 (NEWS 2): Model development and implementation. *Environ. Model. Software* **25**, 837–853 (2010).
60. M. T. H. van Vliet, L. P. H. van Beek, S. Eisner, M. Flörke, Y. Wada, M. F. P. Bierkens, Multi-model assessment of global hydropower and cooling water discharge potential under climate change. *Glob. Environ. Chang.* **40**, 156–170 (2016).
61. Y. Zhao, L. Zhang, Y. Pan, Y. Wang, F. Paulot, D. K. Henze, Atmospheric nitrogen deposition to the northwestern Pacific: Seasonal variation and source attribution. *Atmos. Chem. Phys.* **15**, 10905–10924 (2015).
62. W. Xu, X. S. Luo, Y. P. Pan, L. Zhang, A. H. Tang, J. L. Shen, Y. Zhang, K. H. Li, Q. H. Wu, D. W. Yang, Y. Y. Zhang, J. Xue, W. Q. Li, Q. Q. Li, L. Tang, S. H. Lu, T. Liang, Y. A. Tong, P. Liu, Q. Zhang, Z. Q. Xiong, X. J. Shi, L. H. Wu, W. Q. Shi, K. Tian, X. H. Zhong, K. Shi, Q. Y. Tang, L. J. Zhang, J. L. Huang, C. E. He, F. H. Kuang, B. Zhu, H. Liu, X. Jin, Y. J. Xin, X. K. Shi, E. Z. Du, A. J. Dore, S. Tang, J. L. Collett, K. Goulding, Y. X. Sun, J. Ren, F. S. Zhang, X. J. Liu, Quantifying atmospheric nitrogen deposition through a nationwide monitoring network across China. *Atmos. Chem. Phys., 12360* **15**, 12345 (2015).
63. W. Xu, L. Zhang, X. Liu, A database of atmospheric nitrogen concentration and deposition from the nationwide monitoring network in China. *Sci. Data* **6**, 51 (2019).
64. Y. P. Pan, Y. S. Wang, G. Q. Tang, D. Wu, Wet and dry deposition of atmospheric nitrogen at ten sites in Northern China. *Atmos. Chem. Phys.* **12**, 6515–6535 (2012).
65. Y. Zhang, C. Liu, X. Liu, W. Xu, Z. Wen, Atmospheric nitrogen deposition around the Dongting Lake, China. *Atmos. Environ.* **207**, 197–204 (2019).
66. M. Strokal, Z. Bai, W. Franssen, N. Hofstra, A. A. Koelmans, F. Ludwig, L. Ma, P. van Puijenbroek, J. E. Spanier, L. C. Vermeulen, M. T. H. van Vliet, J. van Wijnen, C. Kroeze, Urbanization: An increasing source of multiple pollutants to rivers in the 21st century. *npj Urban Sustain.* **1**, 24 (2021).
67. Y. Tong, Y. Zhao, G. Zhen, J. Chi, X. Liu, Y. Lu, X. Wang, R. Yao, J. Chen, W. Zhang, Nutrient loads flowing into coastal waters from the main rivers of China (2006–2012). *Sci. Rep.* **5**, 16678 (2015).
68. D. N. Moriasi, J. G. Arnold, M. W. Van Liew, R. L. Bingner, R. D. Harmel, T. L. Veith, Model evaluation guidelines for systematic quantification of accuracy in watershed simulations. *Transac. ASABE* **50**, 885–900 (2007).
69. X. Li, L. Yang, W. Yan, Model analysis of dissolved inorganic phosphorus exports from the Yangtze river to the estuary. *Nutr. Cycl. Agroecosyst.* **90**, 157–170 (2011).
70. X. Liu, A. H. W. Beusen, L. P. H. Van Beek, J. M. Mogollón, X. Ran, A. F. Bouwman, Exploring spatiotemporal changes of the Yangtze River (Changjiang) nitrogen and phosphorus sources, retention and export to the East China Sea and Yellow Sea. *Water Res.* **142**, 246–255 (2018).
71. Y. Tong, X. Bu, J. Chen, F. Zhou, L. Chen, M. Liu, X. Tan, T. Yu, W. Zhang, Z. Mi, L. Ma, X. Wang, J. Ni, Estimation of nutrient discharge from the Yangtze River to the East China Sea and the identification of nutrient sources. *J. Hazard. Mater.* **321**, 728–736 (2017).
72. W. Yan, E. Mayorga, X. Li, S. P. Seitzinger, A. F. Bouwman, Increasing anthropogenic nitrogen inputs and riverine DIN exports from the Changjiang River basin under changing human pressures. *Global Biogeochem. Cycles* **24**, 3575 (2010).
73. Ministry of Water Resources of the People's Republic of China, *Chinese Water Resources Bulletins* (in Chinese) (Ministry of Water Resources of the People's Republic of China, Beijing, 2013).
74. L. Ma, G. L. Velthof, F. H. Wang, W. Qin, W. F. Zhang, Z. Liu, Y. Zhang, J. Wei, J. P. Lesschen, W. Q. Ma, O. Oenema, F. S. Zhang, Nitrogen and phosphorus use efficiencies and losses in the food chain in China at regional scales in 1980 and 2005. *Sci. Total Environ.* **434**, 51–61 (2012).
75. X. Chen, M. Strokal, C. Kroeze, L. Ma, Z. Shen, J. Wu, X. Chen, X. Shi, Seasonality in river export of nitrogen: A modelling approach for the Yangtze River. *Sci. Total Environ.* **671**, 1282–1292 (2019).
76. J. Yang, M. Strokal, C. Kroeze, X. Chen, Z. Bai, H. Li, Y. Wu, L. Ma, Seasonal river export of nitrogen to Guanting and Baiyangdian lakes in the Hai He basin. *J. Geophys. Res. Biogeosci.* **126**, e2020JG005689 (2021).
77. X. Chen, M. Strokal, M. T. H. van Vliet, X. Fu, M. Wang, L. Ma, C. Kroeze, In-stream surface water quality in China: A spatially-explicit modelling approach for nutrients. *J. Clean. Prod.* **334**, 130208 (2022).
78. M. Strokal, V. Strokal, C. Kroeze, The future of the Black Sea: More pollution in over half of the rivers. *Ambio* **52**, 339–356 (2023).
79. V. Strokal, E. J. Kuiper, M. P. Bak, P. Vriend, M. Wang, J. van Wijnen, M. Strokal, Future microplastics in the Black Sea: River exports and reduction options for zero pollution. *Mar. Pollut. Bull.* **178**, 113633 (2022).
80. Y. Li, M. Wang, X. Chen, S. Cui, N. Hofstra, C. Kroeze, L. Ma, W. Xu, Q. Zhang, F. Zhang, M. Strokal, Multi-pollutant assessment of river pollution from livestock production worldwide. *Water Res.* **209**, 117906 (2021).

Acknowledgments

Funding: This work was supported by the National Natural Science Foundation of China (42175137) (to W.X.), National Key Research and Development Program of China (2021YFD1700902 and 2023YFD1702103) (to W.X.), China Scholarship Council (201913043) (to S.F.), the High-level Team Project of China Agricultural University (to Xuejun Liu), and the Beijing Advanced Discipline Funding (to F.Z.). **Author contributions:** W.X., M.W., and Y.Z. designed the study. S.F., W.X., and Xuejun Liu performed the measurements and model simulations. S.F., M.W., and W.X. performed the data analysis and prepared the figures and tables. S.F., W.X., M.W., and M.R.H. wrote the manuscript with comments from Y.Z., M.S., C.K., Xueyan Liu, and F.Z. **Competing interests:** The authors declare that they have no competing interests. **Data and materials availability:** All data needed to evaluate the conclusions in the paper are present in the paper and/or the Supplementary Materials. Source data are provided with this paper.

Submitted 17 March 2024
Accepted 2 August 2024
Published 11 September 2024
10.1126/sciadv.adp2558